Computers and Concrete, *Vol. 25, No. 3* (*2020*) *273-282*
DOI: https://doi.org/10.12989/cac.2020.25.3.273

Effects of diaphragm flexibility on the seismic design acceleration of precast concrete diaphragms

Dichuan Zhang*[1], Robert B. Fleischman[2] and Deuckhang Lee[3]

[1]School of Engineering and Digital Sciences, Nazarbayev University, Kazakhstan
[2]Department of Civil Engineering and Engineering Mechanics, University of Arizona, USA
[3]Department of Architectural Engineering, Chungbuk National University, Korea

(*Received May 18, 2019, Revised February 14, 2020, Accepted February 17, 2020*)

Abstract. A new seismic design methodology for precast concrete diaphragms has been developed and incorporated into the current American seismic design code. This design methodology recognizes that diaphragm inertial forces during earthquakes are highly influenced by higher dynamic vibration modes and incorporates the higher mode effect into the diaphragm seismic design acceleration determination using a first mode reduced method, which applies the response modification coefficient only to the first mode response but keeps the higher mode response unreduced. However the first mode reduced method does not consider effects of diaphragm flexibility, which plays an important role on the diaphragm seismic response especially for the precast concrete diaphragm. Therefore this paper investigated the effect of diaphragm flexibility on the diaphragm seismic design acceleration for precast concrete shear wall structures through parametric studies. Several design parameters were considered including number of stories, diaphragm geometries and stiffness. It was found that the diaphragm flexibility can change the structural dynamic properties and amplify the diaphragm acceleration during earthquakes. Design equations for mode contribution factors considering the diaphragm flexibility were first established through modal analyses to modify the first mode reduced method in the current code. The modified first mode reduced method has then been verified through nonlinear time history analyses.

Keywords: diaphragm flexibility; seismic design; precast concrete diaphragm; modal analysis; nonlinear time history analysis

1. Introduction

A new seismic design methodology (DSDM TG 2014, Ghosh *et al*. 2017, BSSC IT6 2014) for precast concrete diaphragms was developed through multi-university research efforts (Fleischman *et al*. 2013). This design methodology has been codified into the current American seismic design code (ASCE-7 2016) and extended into other construction materials such as reinforced concrete, steel and wood (Zhang *et al*. 2016a). This design methodology recognizes that diaphragm inertial forces during earthquakes are highly influenced by higher dynamic vibration modes. It then incorporates the higher mode effect into the diaphragm seismic design acceleration determination using a first mode reduced method (Rodriguez *et al*. 2012). The first mode reduced method applies the response modification coefficient (*R* factor in ASCE-7) only to the first mode response but keeps the higher mode response unreduced. However, the first mode reduced method does not consider effects of diaphragm flexibility, which plays an important role on the diaphragm seismic response especially for the precast concrete diaphragm (Fleishman and Farrow 2001).

Poor performance during major earthquakes was observed for the precast concrete diaphragm. Especially in the 1994 Northridge earthquake, collapse of several precast concrete parking structures was due to failures of the diaphragm (Iverson and Hawkins 1994). Since then, understanding of the behavior of precast concrete diaphragms has been steadily improved through extensive analytical and experimental research (Oliva 2000, Shaikh and Feile 2004, Naito and Ren 2013, Ren and Naito 2013, Schoettler *et al*. 2009, Tsampras et al. 2016). It has been realized that the dynamic behavior of the precast concrete diaphragm is heavily affected by its flexible nature. During earthquakes, the diaphragm flexibility can lead to: (1) the amplified diaphragm inertial force, even after yielding of the lateral force resisting system (LFRS) (Fleischman *et al*. 2002, Zhang *et al*. 2019); (2) complicated force paths in the diaphragm (Wood *et al*. 2000, Bournas *et al*. 2013, Negro *et al*. 2013, Zhang and Fleischman 2019); (3) non-proportional combined internal forces (Lee and Kuchma 2008, Belleri *et al*. 2014, Farrow and Fleischman 2003, Zhang *et al*. 2011); and (4) amplified inter-story drifts of the gravity columns far away from LFRS (Fleischman *et al*. 1998, Wan *et al*. 2012, Belleri *et al.* 2015, Zhang and Fleischman 2016).

Therefore, this paper investigated the effect of diaphragm flexibility on the diaphragm seismic design acceleration for precast concrete shear wall structures through parametric studies. The main focus was on how the diaphragm flexibility affects the diaphragm seismic design acceleration determined from the 1st mode reduced method.

∗Corresponding author, Assistant Professor
E-mail: dichuan.zhang@nu.edu.kz

http://www.techno-press.org/?journal=cac&subpage=8 ISSN: 1598-8198 (Print), 1598-818X (Online)

Table 1 Structural geometry parameters

Structure #	# of Stories (N)	L_{sw} (m)	t_{sw} (mm)	Structure #	L (m)	d (m)	AR L/d	Floor area (m^2)
1	1	3.66	508	a	Rigid diaphragm			
2	2	4.88	508	b	36.6	45.7	0.8	1672
3	3	6.10	508	c	45.7	36.6	1.3	1672
4	4	7.92	508	d	54.9	30.5	1.8	1672
5	6	9.75	508	e	61.0	27.4	2.2	1672
6	8	10.97	508	f	67.1	24.9	2.7	1672
7	10	12.19	508	g	73.2	22.9	3.2	1672
8	12	13.41	508	h	79.2	21.1	3.8	1672
				i	85.3	19.6	4.4	1672
				j	91.4	18.3	5.0	1672

Table 2. LFRS seismic design

Seismic design coefficient					Wall detail					
#	# of Stories (N)	C_s	T_1 [s]	M_u [1] [kN-m]	Reinforcement End/Web	Reinforcement Space [mm]	ρ	M_y [kN-m]	M_{ult} [2] [kN-m]	Ω_0 [2] / [1]
1	1	0.167	0.144	3295	#8 / #6	152	1.13%	5491	8237	2.5
2	2	0.167	0.255	10982	#8 / #6	152	1.12%	18303	27455	2.5
3	3	0.167	0.356	23062	#8 / #6	152	1.11%	38437	57656	2.5
4	4	0.167	0.400	39535	#8 / #6	152	1.10%	65892	98839	2.5
5	6	0.166	0.603	85946	#8 / #6	152	1.10%	143243	214864	2.5
6	8	0.117	0.853	107799	#8 / #6	152	1.11%	179665	269498	2.5
7	10	0.099	1.104	130858	#8 / #6	152	1.11%	218096	327144	2.5
8	12	0.086	1.351	155232	#8 / #6	152	1.12%	258721	388081	2.5

Several design parameters were considered including number of stories, diaphragm geometries and stiffness. Design equations for mode contribution factors considering the diaphragm flexibility were first established through modal analyses to modify the first mode reduced method in the current code (ASCE-7 2016). The modified first mode reduced method has then been verified through nonlinear time history analyses.

2. Diaphragm seismic design acceleration

In the previous design code (ASCE-7 2010), response modification factor (R) used for the LFRS design is incorrectly applied to the diaphragm, which leads to an underestimation of the diaphragm seismic design acceleration. This underestimation is caused by the fact that the R factor is tied to the fundamental (1st) mode which controls the LFRS response (Eberhard and Sozen 1993) while the diaphragm acceleration demand under earthquakes is tied to higher modes (Rodriguez *et al.* 2002) and not affected by the R factor. Thus, in the new diaphragm design methodology (ASCE-7 2016), the first mode reduced method is used to determine the diaphragm design acceleration (C_{pn}). This method considers the first and higher dynamic vibration modes response. The response modification factor (R) is only applied to the first mode response since the diaphragm higher mode response is not limited by the yielding of LFRS whose design strength are reduced by R.

The diaphragm design acceleration is determined using Eq. (1) according to the current design code. As seen in Eq. (1), the diaphragm design acceleration is a superposition (square root of the sum of squares) of modal responses from the first and higher modes. C_s is the seismic response coefficient (acceleration) for the first mode response, which has been reduced by the R factor from the structural design spectrum response acceleration (S_a) at the first mode period (T_1, Refer to ASCE-7 2016). C_{s2} is the seismic response coefficient (acceleration) for the higher modes response, which is not reduced by the R factor and is conservatively taken as the structural design spectrum response acceleration at short periods (i.e., $S_{DS}=S_a$ @ short periods, plateau of the design acceleration response spectrum). Ω_0 is the overstrength factor for the LFRS. Γ_{m1} and Γ_{m2} are the mode contribution factors for the first and higher modes (square root of the sum of squares from 2nd mode to the last mode), which can be calculated by Eq. (2) and Eq. (3) respectively. The z_s is the mode shape factor for different LFRS (it is taken as 1.0 for shear wall structures) and N is the number of stories. It is noticed from Eqs. (1) to (3) that the diaphragm seismic design acceleration is determined without considering the diaphragm flexibility in the current design code.

$$C_{pn} = \sqrt{(\Gamma_{m1}\Omega_0 C_s)^2 + (\Gamma_{m2} C_{s2})^2} \tag{1}$$

$$\Gamma_{m1} = 1 + \frac{z_s}{2}\left(1 - \frac{1}{N}\right) \tag{2}$$

$$\Gamma_{m2} = 0.9 z_s \left(1 - \frac{1}{N}\right)^2 \tag{3}$$

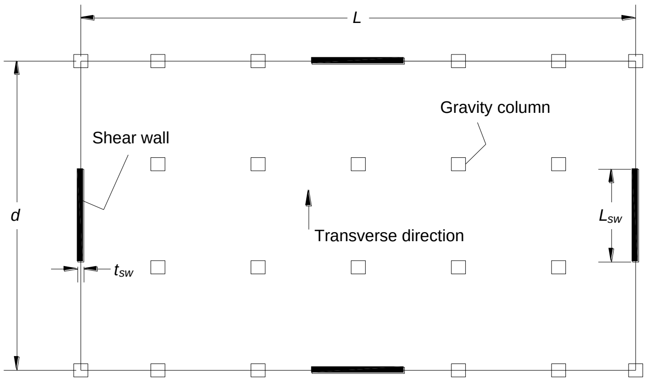

Fig. 1 Plan of prototype structure

3. Parametric study

3.1 Prototype structure

Prototype structure used in this study is a perimeter shear wall building. As seen in Fig. 1, the structure has a footprint of $L \times d$ with different numbers of stories (N). Several combinations of L and d were considered to varying diaphragm geometries as listed in Table 1. The variation of floor plan ($L \times d$) is to represent different diaphragm flexibilities by fixing the total floor area (1672 m^2). Eight different numbers of stories and nine different diaphragm geometries plus a theoretical rigid diaphragm case were studied with a total of 80 structures in combination. The floor-to-floor height is 3.66 m for all stories. The LFRS is perimeter shear wall at each face of the structure. The wall dimensions were preliminary sized for different structural heights as shown in Table 1. The typical floor mass is 6.46 kPa for typical precast concrete structures. Only transverse direction is designed and considered in this study.

3.2 LFRS seismic design

The seismic design of the lateral force resisting system follows the ASCE-7 (2016). A generic design site for the seismic design category D was used with S_s=1.5 and S_1=0.6. Soil class site D was assumed for this study resulting S_{DS}=1.0 and S_{D1}=0.6. The LFRS was adopted as the special precast concrete shear wall with R=6 and Ω_0=2.5. The calculated seismic response coefficients (C_s) for the fundamental (1st) period with rigid diaphragms are shown in Table 2 for different numbers of stories. The longitudinal reinforcement detail, yielding moment (M_y), and ultimate moment (M_{ult}) at the base of the shear wall were designed following the ACI 318 (2014) and are also presented in Table 2.

3.3 Diaphragm flexibility measurement

Diaphragm flexibility index (α) is introduced as the ratio of the shear wall stiffness (k_{sw}) over the diaphragm stiffness (k_{dia}). The shear wall stiffness (k_{sw}) was calculated based on a cantilever wall with the fixed base boundary by considering 65% reduction in the flexure rigidity and 60% reduction in the effective shear area due to possible cracking in the concrete (ACI 318 2014). The diaphragm stiffness (k_{dia}) was calculated based on a simply supported beam under uniformly distributed load by considering 75% reduction in the flexure rigidity and 60% reduction in the effective shear area because the precast concrete diaphragm consists discrete panels connected with reinforcement or hardware rather than a monolithic piece (Wan *et al.* 2015) (Zhang *et al.* 2016b). The stiffness of the shear wall for different numbers of stories and the stiffness of the diaphragm for different structural plans (AR: aspect ratio) are shown in Table 3. By using the stiffness in Table 3, the diaphragm flexibility index (α) was calculated as k_{sw}/k_{dia} for 80 different combinations as shown in Fig. 2. As seen in

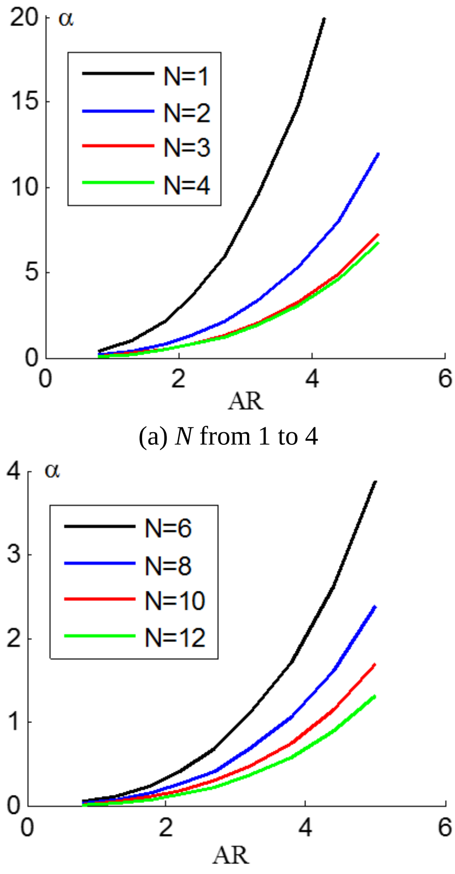

(a) N from 1 to 4

(b) N from 6 to 12

Fig. 2 Diaphragm flexibility index

Table 3 Stiffness of the LFRS and diaphragm

#	N	k_{sw} [kN/m]	#	AR L/d	k_{dia} [kN/m]
1	1	175402	a	Rigid	∞
2	2	62547	b	0.8	415616
3	3	38091	c	1.3	184269
4	4	35513	d	1.8	82097
5	6	20375	e	2.2	48793
6	8	12526	f	2.7	29665
7	10	8906	g	3.2	18503
8	12	6911	h	3.8	11847
			i	4.4	7779
			j	5.0	5231

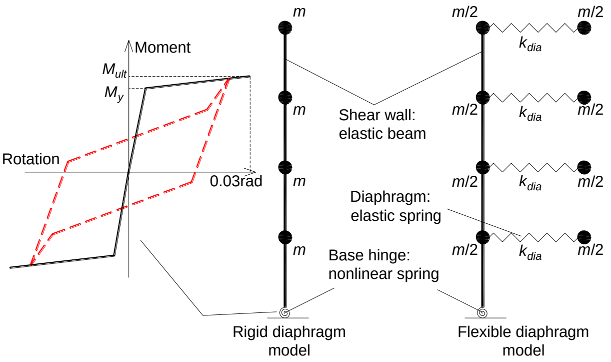

Fig. 3 Structural models

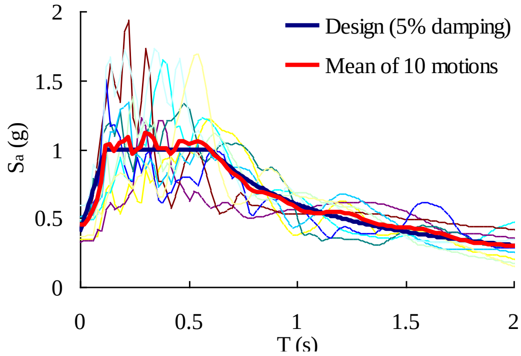

Fig. 4 Acceleration response spectrum for ground motions

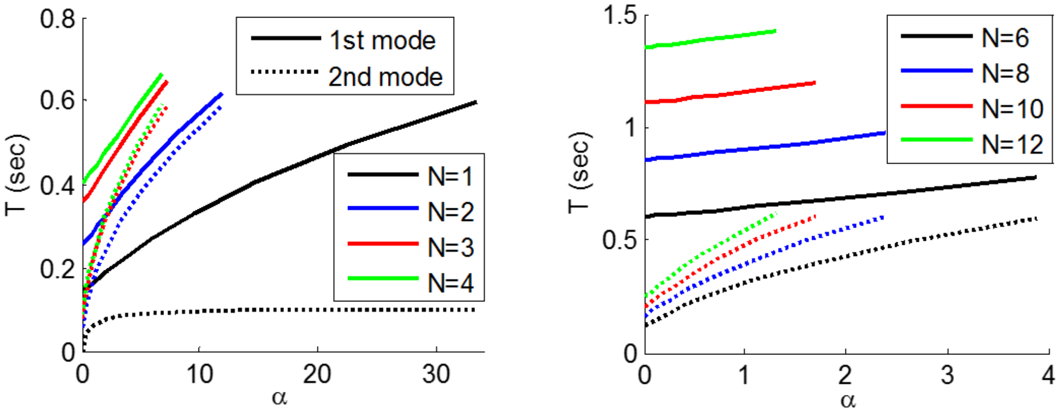

(a) *N* from 1 to 4 (b) *N* from 6 to 12

Fig. 5 Structural periods

Fig. 2, the diaphragm flexibility index increases as the increase of the AR but reduces as the increase of the *N* due to the decrease of the shear wall stiffness (Refer to Table 3).

4. Analytical modeling

4.1 Structural models

Simplified structural models were used for both rigid and flexible diaphragms as shown in Fig. 3 since the main focus of this study is on the diaphragm global demand rather than the local diaphragm seismic response. These simplified models are able to reasonably capture the diaphragm global behavior under earthquakes as compared to more sophisticate models and test results (Zhang 2010). As seen in Fig. 3, the shear wall was modeled as an elastic beam element with base hinge (nonlinear rotational spring) which represents seismic behavior of typical precast concrete walls. For the rigid diaphragm model, the structural mass (*m*) was rigidly attached to the shear wall at each floor level. For the flexible diaphragm model, half of the structural mass (m/2) was assigned to the shear wall and to the diaphragm respectively. The diaphragm flexibility was modeled as elastic springs with the stiffness of k_{dia} listed in Table 3. The gravity columns were ignored.

Two types of analyses were conducted: (1) modal analysis; (2) nonlinear time history analysis. The modal analysis was performed using the simplified models shown in Fig. 3 with removal of the nonlinear spring at the base of the shear wall. The nonlinear time history analysis was conducted directly using the simplified models shown in Fig. 3 with a 5% Rayleigh damping. The damping constant was calculated to anchor the first and third modes at designated damping ratio (5%). Thus, the second mode conservatively has a lower damping ratio than 5%. The integration time step was conducted at 1/400 sec. The output time step was set as 1/100 sec.

4.2 Ground motion inputs

A suite of ten historical earthquakes was used for the nonlinear time history analysis. These earthquakes were selected from the 44 far field set of ground motions proposed by FEMA-P695. The ground motions from these earthquakes were scaled to have the mean of 10 motions matching the 5% damping design acceleration response spectrum as seen in Fig. 4. The nonlinear time history analyses were performed at the design basis level earthquake. Mean results from the 10 ground motions will be presented.

5. Analytical results

5.1 Modal analyses

The modal analyses conducted in this study investigate

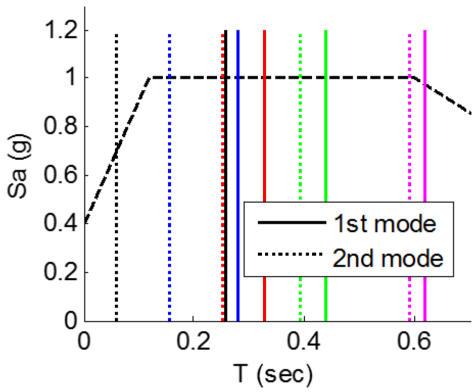

(a) N=6

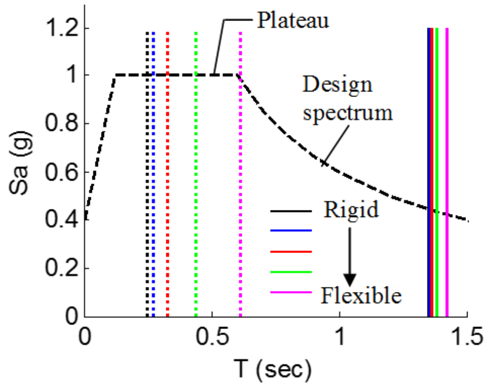

(b) N=12

Fig. 6 Design acceleration response spectrum with structural period indications

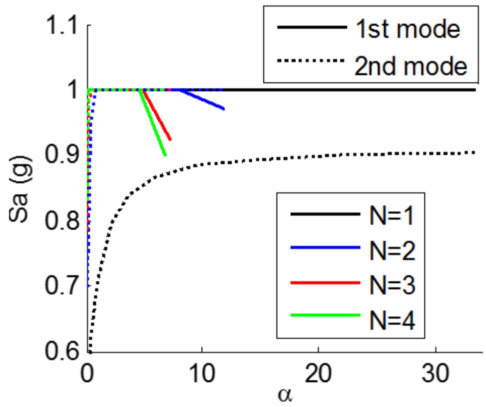

(a) N from 1 to 4

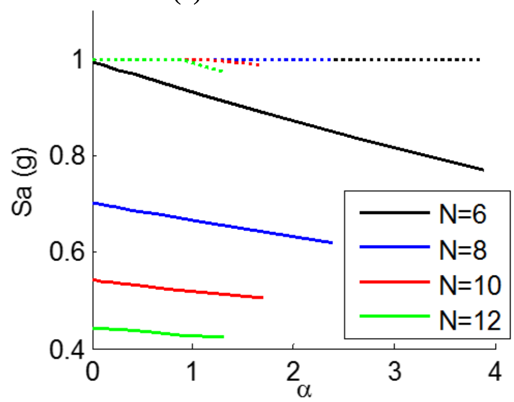

(b) N from 6 to 12

Fig. 7 Structural design spectrum acceleration response

the effect of the diaphragm flexibility on the structural periods (T), design spectrum response accelerations (S_a) and mode contribution factors (Γ_m) since the current diaphragm seismic design acceleration is depended on these factors as indicated in Eq. (1).

Fig. 5 shows the structural periods at the 1st and 2nd modes vs. the diaphragm flexibility index for different numbers of stories. As seen in Fig. 5, the diaphragm flexibility significantly elongates the structural period for both 1st and 2nd modes. The elongation rate is higher in the 2nd mode than that of the 1st mode as the diaphragm flexibility increases. The elongation of the structural periods will in turn change the structural design spectrum response acceleration (S_a) at corresponding mode periods. Fig. 6 shows the design acceleration response spectrum with the structural 1st and 2nd mode periods indications for 2-story and 12-story structures. As seen in Fig. 6(a), as the structural periods elongate, the coordinates of the 1st mode and 2nd mode on the spectrum does not change significantly. Only for rigid diaphragm, the coordinates of the 2nd mode may fall in the ascending branch; while for highly flexible diaphragm, the coordinates of the 1st mode may fall in the descending branch. As seen in Fig. 8(b), as the structural periods elongate, the coordinates of the 1st mode on the spectrum reduces while the coordinate of the 2nd mode remains on the plateau.

Fig. 7 summarizes the design spectrum response acceleration (S_a) for 1st and 2nd modes vs. the diaphragm flexibility index for different numbers of stories. As seen in Fig. 7, the 1st mode design acceleration changes as the diaphragm flexibility increases especially more significant for tall buildings (N>6). For tall buildings, the 2nd mode design acceleration remains nearly the same at the plateau of the design spectrum; while for short buildings, it increases rapidly from the ascending branch to the plateau as the diaphragm flexibility increases. Thus, it is more rationale to align the C_s value in design Eq. (1) to the design spectrum response acceleration at the structural 1st mode period with the diaphragm flexibility in consideration. On the other hand, it is conservative and reasonable to keep the C_{s2} value in design Eq. (1) at the plateau of the design spectrum (i.e., S_{DS}) regardless of the diaphragm flexibility.

Fig. 8 shows the mode contribution factors (Γ_m) for the 1st and higher modes vs. the diaphragm flexibility index for different numbers of stories. As seen in Fig. 8, the diaphragm flexibility tends to amplify the modal response to a point and then starts to reduce the modal response possibly because the dynamic response between the LFRS and the diaphragm starts to isolate each other when the diaphragm becomes highly flexible. However, overall the flexible diaphragm has the higher modal response than the rigid diaphragm at α=0. In general, the higher mode response has the isolation effect earlier than the 1st mode response as the diaphragm flexibility increases.

Since the diaphragm flexibility changes the modal response and the corresponding mode contribution factor, it is important to update the Eqs. (2) and (3) to include proper diaphragm flexibility effects. The first step is to normalize

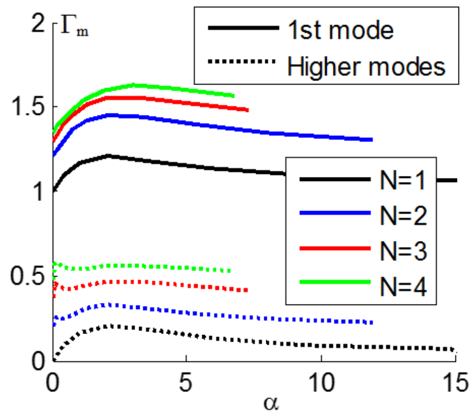

(a) N from 1 to 4

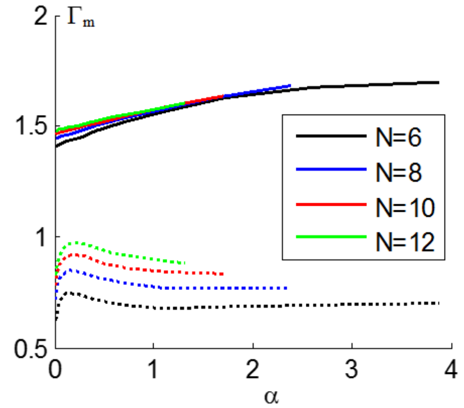

(b) N from 6 to 12

Fig. 8 Mode contribution factors

the mode contribution factor (Γ_m) by the one with the rigid diaphragm (α=0) except for the higher modes in the 1-story structure where the Γ_{m2}=0 at α=0. Figs. 9(a) and (b) show the normalized mode contribution factor for the 1st (Γ_{m1}) and higher (Γ_{m2}) modes respectively for all structures considered in this study except for Γ_{m2} of the 1-story structure; while Fig. 9(c) shows the Γ_{m2} for the 1-story structure. As seen in Fig. 9, the variation trend of the modal contribution factor over the diaphragm flexibility is similar for structures with different numbers of stories. Four new parameters were introduced: MF_1, MF_2, Γ_{mf1} and Γ_{mf2}. MF_1 and MF_2 represent the normalized mode contribution factor for the 1st and higher modes respectively. Γ_{mf1} and Γ_{mf2} represent the mode contribution factor with the diaphragm flexibility in consideration for the 1st and higher modes respectively. Equations for MF_1, MF_2 and Γ_{mf2} (N=1) were developed to fit the data in Fig. 9 shown as red solid lines

$$MF_1=\frac{\Gamma_{m1}}{\Gamma_{m1@\alpha=0}}=\begin{cases}1+0.22\left[\dfrac{5\alpha/3-(\alpha/3)^2}{(1+\alpha)}\right], & \alpha\le 12\\ -0.028\ln(\alpha)+1.137, & \alpha>12\end{cases}\tag{4}$$

$$MF_2=\frac{\Gamma_{m2}}{\Gamma_{m2@\alpha=0}}=\begin{cases}1+0.22\left[\dfrac{13\alpha/0.15-(\alpha/0.15)^2}{(1+11\alpha/0.15)}\right], & \alpha\le 1.5\\ -0.028\ln(\alpha)+1.071, & \alpha>1.5\end{cases}\tag{5}$$

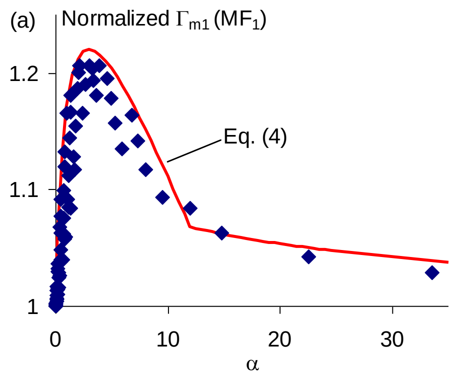

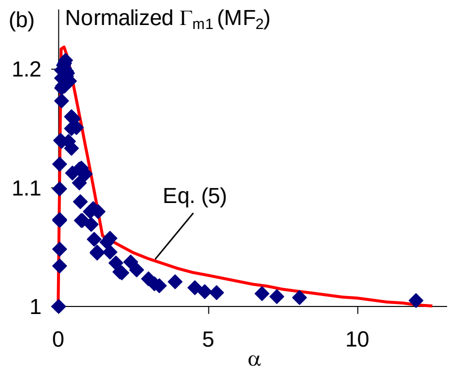

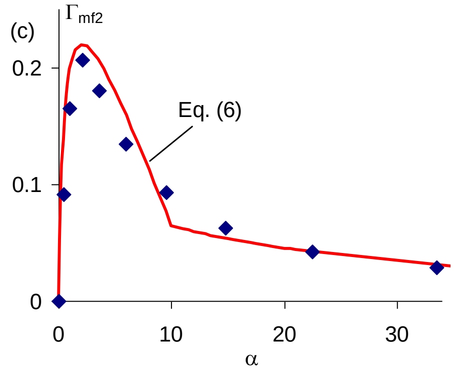

Fig. 9 Normalized mode contribution factors: (a) 1st mode; (b) higher modes; (3) higher modes for N=1

$$\Gamma_{mf2}(N=1)=\begin{cases}0.22\left[\dfrac{6\alpha/2.1-(\alpha/2.1)^2}{(1+4\alpha/2.1)}\right], & \alpha\le 10\\ -0.028\ln(\alpha)+0.129, & \alpha>10\end{cases}\tag{6}$$

Using Eqs. (4) and (5), the equations for the mode contribution factors with the diaphragm flexibility in consideration can be developed on the basis of the Eqs. (2) and (3)

$$\Gamma_{mf1}=(MF_1)\Gamma_{m1}\quad\text{(for all structures)}\tag{7}$$

$$\Gamma_{mf2}=(MF_2)\Gamma_{m2}\quad\text{(for structures with } N\text{>1)}\tag{8}$$

Fig. 10 shows the comparison of the mode contribution factors from the modal analysis with those calculated from Eqs. (6) to (8) for the different diaphragm flexibilities. As seen in the Fig. 10, the proposed equations reasonably match the analysis results. Thus it is proposed to modify the equation for the diaphragm seismic design acceleration (Eq.

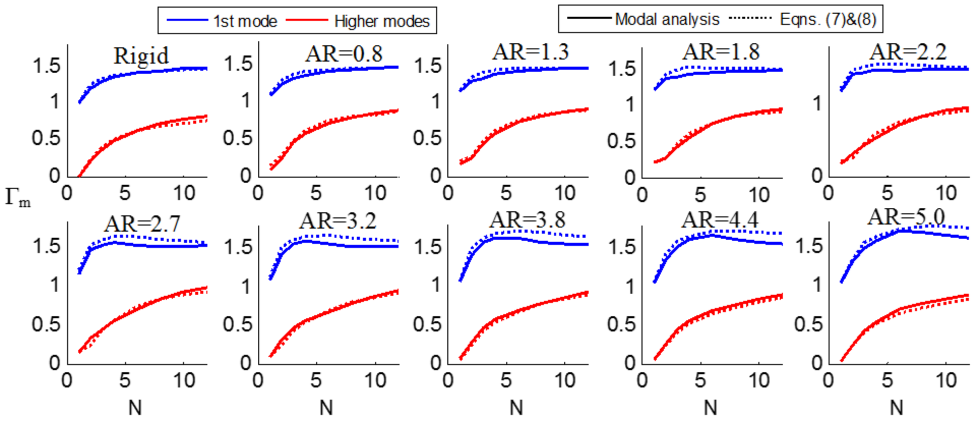

Fig. 10 Mode contribution factors comparison

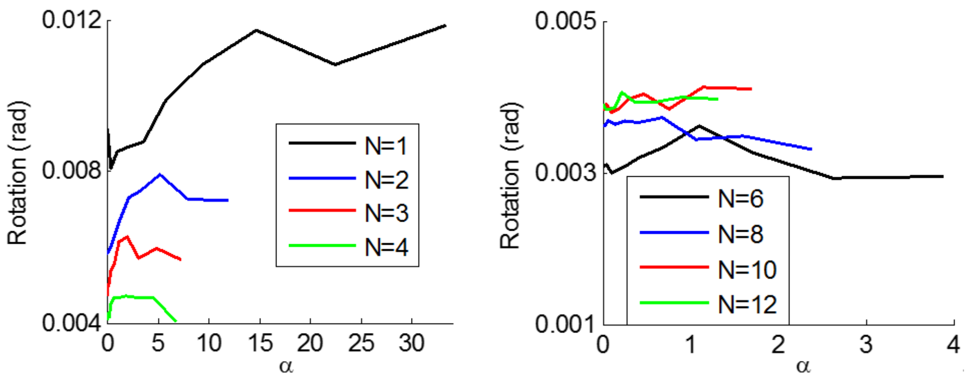

(a) *N* from 1 to 4 (b) *N* from 6 to 12

Fig. 11 Shear wall rotation response

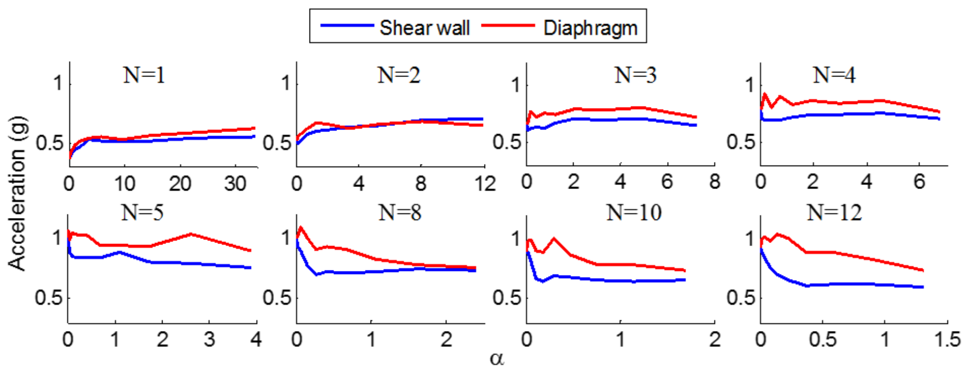

Fig. 12 Maximum acceleration demand

(1)) to include the effect of the diaphragm flexibility as the follow

$$C_{pn} = \sqrt{(\Gamma_{mf1}\Omega_0 C_s)^2 + (\Gamma_{mf2} C_{s2})^2} \qquad (9)$$

where Γ_{mf1} and Γ_{mf2} can be calculated using Eqs. (6) to (8); C_s can be calculated based on the structural 1st mode period including the diaphragm flexibility; other factors will remain unchanged from the current design code (ASCE-7 2016).

5.2 Nonlinear time history analyses

This section presents the results from the nonlinear time history analysis. The modified diaphragm seismic design acceleration equation (Eq. (9)) will also be verified using the results from the analysis.

Fig. 11 shows the maximum plastic rotation at the base of the shear wall. It indicates that the structure has gone through the expected nonlinear response in the LFRS (less than 0.015 according to ASCE-7 2016), which is important before examining the diaphragm response. In general, the plastic rotation demand increases as the diaphragm flexibility increases especially for short buildings.

Fig. 12 shows the maximum acceleration demand at the shear wall and the diaphragm. As seen in the Fig. 12, the diaphragm acceleration demand is larger than the shear wall acceleration demand for the flexible diaphragm. The

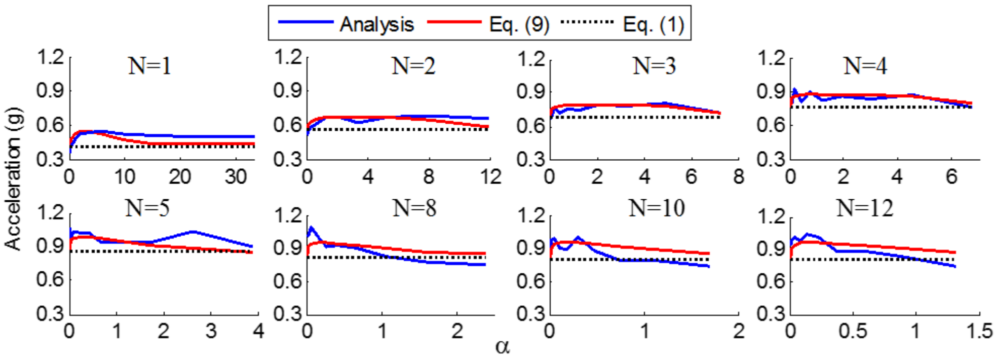

Fig. 13 Maximum diaphragm acceleration demand comparison

diaphragm flexibility tends to amplify the diaphragm acceleration to a point and then starts to reduce due to the isolation effect as discussed previously. This trend is consistent with the one for the mode contribution factor observed in the modal analysis (refer to Fig. 8). The amplification effect is more significant for the tall buildings than the short buildings.

Fig. 13 shows the comparison of the diaphragm acceleration obtained from maximum demand in the nonlinear time history analysis, modified diaphragm seismic design acceleration Eq. (9), and the current diaphragm seimic design acceleration Eq. (1). As seen, the modified design equation can reasonably capture the demand obtained from the nonlinear time history analysis and reflect the diaphragm flexibility amplificaiton effect on the diaphragm acceleration demand during earthquakes.

6. Conclusions

This paper investigated the effect of the diaphragm flexibility on the diaphragm seismic response and design acceleration for the precast concrete diaphragm. Modal analyses were first conducted to investigate the dynamic properties under the influence of the diaphragm flexibility. Based on the modal analysis results, modified diaphragm seismic design acceleration equation was proposed. This proposed equation was then verified from the results of nonlinear time history analyses. The following conclusions can be made based on the results from the modal and nonlinear time history analysis:

(1) Diaphragm flexibility elongates the structural periods. This elongation has a significant effect on the design spectrum response acceleration at the 1st mode period.

(2) Diaphragm flexibility tends to amplify the diaphragm acceleration demand to a point and then starts to reduce the demand due to possible isolation effect when the diaphragm becomes highly flexible. This trend was observed in the mode contribution factor from the modal analysis and the maximum diaphragm acceleration demand from the nonlinear time history analysis.

(3) The amplification effect of the diaphragm flexibility on the diaphragm acceleration demand is more significant for the tall buildings compared to the short buildings.

(4) The proposed equation for the diaphragm seismic design acceleration can reasonably capture the maximum diaphragm acceleration demand from the nonlinear time history analysis, and can properly reflect the effect of diaphragm flexibility.

The study presented in this paper was conducted using a simplified multi-degree freedom model. The model can predict the diaphragm global response and demand which is suitable for developing the code design equations. However, the simplified model cannot capture the diaphragm local dynamic response which might affect the overall structural dynamic behavior. Therefore, further research is recommended on the diaphragm flexibility for using a more sophisticated structural model.

Acknowledgments

This research was supported by the Precast/Prestressed Concrete Institute (PCI), the Charles Pankow Foundation, and the National Science Foundation (NSF) under Grant CMS-0324522 and SGER Supplement CMMI-0623952. The authors are grateful for this support. Any opinions, findings, and conclusions or recommendations expressed in this material are those of the author(s) and do not necessarily reflect the views of the National Science Foundation.

References

ACI 318-14 (2014), Building Code Requirements for Structural Concrete and Commentary, ACI committee 318.

ASCE 7-10 (2010). Minimum Design Loads for Buildings and Other Structures, American Society of Civil Engineers.

ASCE 7-16 (2016). ASCE Minimum Design Loads and Associated Criteria for Buildings and Other Structures, American Society of Civil Engineers.

Belleri, A., Moaveni, B. and Restrepo, J.I. (2014), "Damage assessment through structural identification of a three-story large-scale precast concrete structure", *Earthq. Eng. Struct. Dyn.*, **43**(1), 61-76. https://doi.org/10.1002/eqe.2332.

Belleri, A., Torquati, M., Riva, P. and Nascimbene, R. (2015), "Vulnerability assessment and retrofit solutions of precast industrial structures", *Earthq. Struct.*, **8**(3), 801-820. http://dx.doi.org/10.12989/eas.2015.8.3.801.

Bournas, D.A., Negro, P. and Molina, F.J. (2013), "Pseudodynamic tests on a full-scale 3-storey precast concrete building: behavior of the mechanical connections and floor diaphragms", *Eng. Struct.*, **57**, 609-627. https://doi.org/10.1016/j.engstruct.2013.05.046.
Building Seismic Safety Council, Committee IT6 (2014), Precast Concrete Diaphragm Design, Proposal IT06-002-Revise ASCE/SEI 7-10 Sections 14.2.4, NEHRP.
DSDM Project Task Group (2014), Seismic Design Methodology Document for Precast Concrete Diaphragms, Project 08-07 Research Product, Charles Pankow Foundation.
Eberhard, M.O. and Sozen, M.A. (1993) "Behavior-based method to determine design shear in earthquake-resistant walls", *ASCE J. Struct. Eng.*, **119**, 619-640. https://doi.org/10.1061/(ASCE)0733-9445(1993)119:2(619).
Farrow, K.T. and Fleischman, R.B. (2003) "Effect of dimension and detail on the capacity of precast concrete parking structure diaphragms", *PCI J.*, **48**(5), 46-61.
Fleischman, R.B. and Farrow, K.T. (2001), "Dynamic response of perimeter lateral-system structures with flexible diaphragms", *Earthq. Eng. Struct. Dyn*., **30**(5), 745-763.
Fleischman, R.B., Farrow, K.T. and Eastman, K. (2002) "Seismic response of perimeter lateral-system structures with highly flexible diaphragms", *Earthq. Spectra*, **18**(2), 251-286.
Fleischman, R.B., Restrepo, J.I., Naito, C.J., Sause, R., Zhang, D. and Schoettler, M. (2013), "Integrated analytical and experimental research to develop a new seismic design methodology for precast concrete diaphragms", *J. Struct. Eng.*, **139**(7), 1192-1204. https://doi.org/10.1061/(ASCE)ST.1943-541X.0000734.
Fleischman, R.B., Sause, R., Pessiki, S. and Rhodes, A.B. (1998), "Seismic behavior of precast parking structure diaphragms", *PCI J.*, **43**(1), 38-53.
Ghosh, S.K., Cleland, N.M. and Naito, C.J. (2017), "Seismic design of precast concrete diaphragms", NEHRP Seismic Design Technical Brief No. 13.
Iverson, J.K. and Hawkins, N.M. (1994), "Performance of precast/prestressed concrete building structures during Northridge Earthquake", *PCI J.*, **39**(2), 38-55.
Lee, H.J. and Kuchma, D.A. (2008), "Seismic response of parking structures with precast concrete diaphragms", *PCI J.*, **53**(2), 71-94.
Naito, C. and Ren, R. (2013), "An evaluation method for precast concrete diaphragm connectors based on structural testing", *PCI J.*, **58**(2), 106-118.
Negro, P., Bournas, D.A. and Molina, F.J. (2013), "Pseudodynamic tests on a full-scale 3-storey precast concrete building: global response", *Eng. Struct.*, **57**, 594-608. https://doi.org/10.1016/j.engstruct.2013.05.047.
Oliva, M.G. (2000), "Testing of the JVI flange connector for precast concrete double-Tee system", Structures and Materials Test Laboratory, College of Engineering, University of Wisconsim, Madison, WI, June.
Ren, R. and Naito, C. (2013), "Precast concrete diaphragm connector performance database", *ASCE J. Struct. Eng.*, **139**(1), 15-27. https://doi.org/10.1061/(ASCE)ST.1943-541X.0000598.
Rodriguez, M., Restrepo, J.I. and Carr, A.J. (2002), "Earthquake induced floor horizontal accelerations in buildings", *Earthq. Eng. Struct. Dyn.*, **31**(3), 693-718. https://doi.org/10.1002/eqe.149.
Schoettler, M.J., Belleri, A., Zhang, D., Restrepo, J. and Fleischman, R.B. (2009), "Preliminary results of the shake-table testing for development of a diaphragm seismic design mythology", *PCI J.*, **54**(1), 100-124.
Shaikh, A.F. and Feile, E.P. (2004), "Load testing of a precast concrete double-tee flange connector", *PCI J.*, **49**(3), 84-95.
Tsampras, G., Sause, R., Zhang, D., Fleischman, R., Restrepo, J., Mar, D. and Maffei, J. (2016), "Development of deformable connection for earthquake-resistant buildings to reduce floor accelerations and force responses", *Earthq. Eng. Struct. Dyn.*, **45**(9), 1473-1494.
Wan, G., Fleischman, R.B. and Zhang, D. (2012), "Effect of spandrel beam to double tee connection characteristic of flexure-controlled precast diaphragms", *ASCE J. Struct. Eng.*, **138**(2), 247-258. https://doi.org/10.1061/(ASCE)ST.1943-541X.0000426.
Wan, G., Zhang, D., Fleischman, R.B. and Naito, C.J. (2015), "A coupled connector element for nonlinear static pushover analysis of precast concrete diaphragms", *Eng. Struct.*, **86**(1), 58-71. https://doi.org/10.1016/j.engstruct.2014.12.029.
Wood, S.L., Stanton, J.F. and Hawkins, N.M. (2000), "New seismic design provisions for diaphragms in precast concrete parking structures", *PCI J.*, **45**(1), 50-65.
Zhang, D. (2010), "Examination of precast concrete diaphragm seismic response by three-dimensional nonlinear dynamic analyses", Ph.D. Dissertation, Univ. of Arizona, Tucson, AZ.
Zhang, D. and Fleischman, R.B. (2016), "Establishment of performance-based seismic design factors for precast concrete floor diaphragms", *Earthq. Eng. Struct. Dyn.*, **45**, 675-698. https://doi.org/10.1002/eqe.2679.
Zhang, D. and Fleischman, R.B. (2019), "Verification of diaphragm seismic design factors for precast concrete parking structures", *Struct. Eng. Mech.*, **71**(6), 643-656. https://doi.org/10.12989/sem.2019.71.6.643.
Zhang, D., Fleischman, R. and Shon, C. (2016a). "Preliminary analytical study on seismic ductility demand of wood diaphragms", *Adv. Struct. Eng.*, **19**(1), 104-115. https://doi.org/10.1177/1369433215622874.
Zhang, D., Fleischman, R.B., Naito, C. and Ren, R. (2011), "Experimental evaluation of pretopped precast diaphragm critical flexure joint under seismic demands", *ASCE J. Struct. Eng.*, **137**(10), 1063-1074. https://doi.org/10.1061/(ASCE)ST.1943-541X.0000352.
Zhang, D., Fleischman, R.B., Naito, C.J. and Zhang, Z. (2016b), "Development of diaphragm connector elements for three-dimensional nonlinear dynamic analysis of precast concrete structures", *Adv. Struct. Eng.*, **19**(2), 187-202. https://doi.org/10.1177/1369433215624319.
Zhang, D., Fleischman, R.B., Schoettler, M.J., Restrepo, J.I. and Mielke, M. (2019), "Precast diaphragm response in a half-scale shake table test", *ASCE J. Struct. Eng.*, **145**(5), 04019024. https://doi.org/10.1061/(ASCE)ST.1943-541X.0002304.

CC

Notations

AR	= diaphragm aspect (span to depth) ratio;
C_{pn}	= diaphragm design acceleration;
C_s	= seismic response coefficient (acceleration) for the 1st mode response;
C_{s2}	= seismic response coefficient (acceleration) for the higher modes response;
d	= diaphragm depth;
k_{dia}	= diaphragm stiffness;
k_{sw}	= shear wall stiffness;
L	= diaphragm span;
L_{sw}, t_{sw}	= depth, thickness of shear wall;
MF_1, MF_2	= normalized mode contribution factor for 1st, higher modes;

M_u	= design moment at the wall base;
M_{ult}	= ultimate moment strength at the wall base;
M_y	= yield moment strength at the wall base;
m	= structural mass;
N	= number of stories;
R	= response modification coefficient;
S_1, S_S	= mapped acceleration parameter at short periods, period of 1.0s;
S_a	= structural design spectrum response acceleration;
S_{DS}	= structural design spectrum response acceleration at short periods;
S_{D1}, S_{DS}	= design acceleration parameter at short periods, period of 1.0s;
T	= structural period;
T_1	= 1st mode period;
z_s	= mode shape factor;
α	= diaphragm flexibility index;
Γ_{m1}, Γ_{m2}	= mode contribution factor for 1st mode, higher modes;
Γ_{mf1}, Γ_{mf2}	= mode contribution factor for 1st mode, higher modes;
ρ	= reinforcement ratio for the shear wall;
Ω_0	= overstrength factor for the LFRS.